# DETERMINATION OF THE SIZE OF REPRESENTATIVE VOLUME ELEMENTS FOR DISCONTINUOUS FIBRE COMPOSITES

C. Qian, L.T. Harper*, T. A. Turner, S. Li, N. A. Warrior
Division of Mechanics, Materials and Structures, The University of Nottingham,
University Park, Nottingham, NG7 2RD
* Corresponding author (lee.harper@nottingham.ac.uk)

## 1 Introduction

Discontinuous fibre composites can be rapidly manufactured using automated processes, with low production costs compared with textile reinforcements [1]. The level of flexibility offered by discontinuous fibre composites can however make efficient design challenging, as additional material and process parameters complicate material selection and quality can be difficult to control compared with textiles. Part consistency can be poor and local material variability can be high [2, 3] if the wrong material parameters are chosen, leading to over conservative safety factors. Predictive models are considered to be important for reducing the level of costly experimental testing during screening and to drive future process and material developments.

Developments in high performance computing have seen an increase in the use of numerical techniques such as Finite Element Analysis (FEA), to model the response of randomly distributed fibre composites. This approach is well documented for studying the transverse response of randomly distributed filaments [4, 5] or spherical inclusions [6] at the micro-scale, but is not so common for modelling 3D randomly packed fibres at the meso-scale. These architectures are far more challenging to model with many more independent variables to consider, particularly for high fibre volume fractions and large aspect ratio fibres [7].

This paper presents a novel method for meshing discontinuous fibre architectures for FEA, which removes many of the limitations imposed by conventional approaches. A random adsorption model has been used to generate architectures in order to study the influence of two different boundary condition strategies on a range of cells containing randomly distributed fibres.

## 2 RVE Generation for Random Fibre.

A representative volume element (RVE) is often used to simulate the behavior of heterogeneous materials. A RVE should be a volume of heterogeneous material that is sufficiently large to be statistically representative, ensuring a sample is taken of all micro-structural heterogeneities that occur in the composite [8]. There are three main methods for creating numerical RVEs for random fibre architectures, which include random sequential adsorption (RSA), Monte Carlo (MC) procedures and image reconstruction [7]. For conventional RSA and MC, fibres are often modelled as thin rods without curvature and fibre-fibre contact is not permitted. The major problem with RSA and MC type approaches is that ‘jamming’ occurs as the fibre content increases, which limits the maximum fibre volume fraction. Modified RSA approaches [7] have enabled the maximum allowable volume fraction to be increased, but they tend to produce unnatural fibre architectures, by either introducing excessive local curvature at fibre cross-over points, or by using a range of fibre diameters to improve packing.

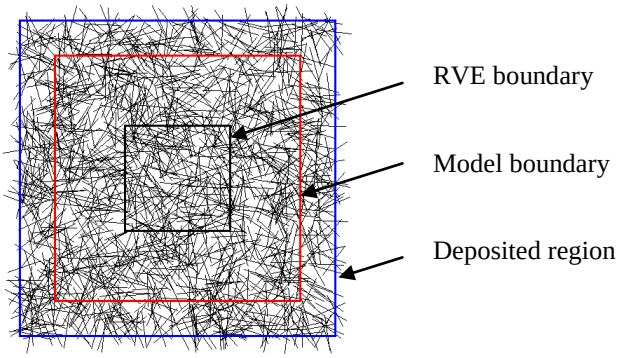


**Fig. 1 Schematic of random sequential adsorption model.**

A modified RSA is adopted in the current paper, and is programmed in Visual Basic® to generate 2D fibre architectures. Fibres are deposited within a region bounded by Cartesian coordinates (Fig. 1). Random numbers are generated for the x-y coordinates of the centre of mass for each fibre, and a third number is used to determine the fibre orientation. This 2D model allows intersecting fibres, thus removing the fibre volume fraction limitation. Moreover, this 2D approach is computationally inexpensive, therefore is practical for simulating larger specimens.

## 3 Finite Element Modelling

Fibre architectures are meshed suitably for processing by ABAQUS/Standard. The matrix material is modelled using structural 2D, plane stress continuum elements (CPS8R). One dimensional beam elements (B22) with circular cross-section are used to represent the fibre bundles, where the diameter is assigned as a function of the filament count and tow volume fraction ($V_{tow}$). The internal structure of each bundle contains resin, and therefore the volume of deposited bundles ($V_{deposited}$) is adjusted to satisfy the target volume fraction of the laminate (Vf):

$$V_{deposited} = \frac{V_f}{V_{tow}} \qquad (1)$$

Beam elements are constrained to the continuum matrix elements using the ABAQUS built-in function *EMBEEDED ELEMENT. This technique eliminates the extra degree of freedom on the embedded elements (fibres) compared with the host elements (matrix) and provides a multi-point constraint. Consequently regular shaped meshes can be used to model the matrix material, without node sharing between beam (fibre) and continuum (matrix) elements. Following [9], the modelling parameters used for the epoxy resin are 3350MPa for tensile modulus and 0.38 for Poisson's ratio. The fibre modulus is 144000MPa. All models are 3.5mm thick and consist of 24K fibre tows with 60% tow volume fraction.

A conventional meshing approach has been used to validate the novel embedding technique, using an unstructured free mesh with coincident nodes at the fibre/matrix interface. Fig. 2 demonstrates the effect of using the *EMBEDDED ELEMENT technique versus using the *TIE command, assuming perfect interfacial bonding in both cases. The edge length of the matrix elements in the embedded model is 0.2mm, which is the same as the length of each beam element. The model is subjected to tensile loading in the horizontal (x) direction. Fig. 2 shows that the stress fields and the displaced shapes are identical for the two meshing approaches.

Comparisons are made with tensile boundary conditions in both horizontal and vertical directions, and in-plane shear is also considered. It is commonly found that there is less than 1% error between the two approaches when comparing the in-plane moduli and Poisson's ratios. It is understood that this meshing method is only an approximation, but the low errors are considered to be acceptable in the current context, since it eliminates problems with mesh density and distorted elements around fibre crossover points.

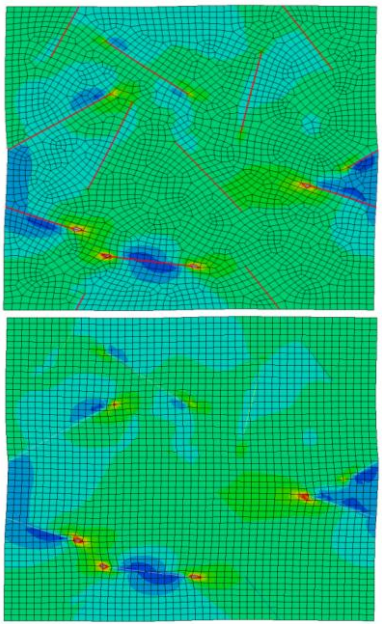

**Fig. 2 Von-Mises stress comparison between a model using an unstructured mesh with tie constraints (top) compared with structured embedded elements (bottom). (Both images are scaled to the same peak stress). Deformation factor is 15 in both cases.**

## 4 Boundary Conditions

Boundary conditions are difficult to derive for random heterogeneous fibre composites and also have a large impact on the RVE generation. It is common to see periodic conditions imposed [10, 11], where the inhomogeneous material is approximated by an infinitely extended model material with a periodic phase arrangement. However, enforcing

periodicity for long slender fibres with larger aspect ratios influences the local fibre volume fraction distribution around the edge of the model, which can affect the critical size of the RVE[12].

According to St Venant's principle [28], the effects of incorrectly prescribed boundary conditions affect only a limited zone next to the boundary. An approximation to the exact solution can be found if a sub-domain is extracted from the model at some critical 'decay length' away from the boundary [13].

An alternative approach uses an embedded cell to avoid imposing periodicity [14, 15], where a core region is embedded in a homogeneous material that simply transmits the applied load [30]. It allows the core to be studied at a high spatial resolution, but similar to the periodic approach, embedding causes perturbations in the local stress and strain fields at the boundary of the core.

Two modelling approaches are investigated in the current paper; using St Venant's principle to establish the 'critical decay length' of incorrectly prescribed periodic boundary conditions. This is achieved by extracting the stress/strain field from an inner cell whose boundaries are the decay length away from of the model boundaries. One of the modelling approaches, named here as the *heterogeneous* approach, consists of fibres within the entire model. For the other approach, named the *homogenous* approach, fibres only exist within the inner RVE cell, and homogeneous material properties are signed to the gap between the two boundaries.

All cells are subjected to periodic boundary conditions, assuming translational symmetries in the x and y directions. The average stress and strain calculations have been implemented into a Python script within ABAQUS/CAE in order to calculate the effective moduli. In principal, stress and strain values should be calculated as volume averaged quantities considering all the fibre and resin elements, however due to the strain compatibility between the resin and the fibre during embedding; only the average strain within resin elements is considered, which can be expressed as:

$$\varepsilon_x^{ave} = \frac{1}{V}\int \varepsilon_x^{resin}\, dV \qquad (2)$$

where x denotes the tensor component corresponding to the load case.

When calculating the stress, both fibre and resin contributions need to be considered:

$$\sigma_x^{ave} = \frac{1}{V}\left(\int \sigma_x^{resin}\, dV + \int \sigma_x^{resin}\, dV\right) \qquad (3)$$

## 5 Mesh Sensitivity Analysis

The influence of varying finite element mesh density on the stress/strain distribution within the model is studied using embedded elements. The same length is used for the beam elements and the side length of the continuum elements, which gradually decreases from 2mm to 0.0125mm. The fibre architecture produced by the RVE generator remains constant for each fibre volume fraction studied. A 20x20mm model is used for each case.

Fig. 3 indicates that the average RVE stress takes longer to converge for higher fibre volume fractions. A greater number of embedded beam elements share the same host elements at higher volume fractions; therefore the mesh needs to be finer to account for a greater number of bundle ends and crossover points. This would also be true for coupons of increasing thickness because of the planar 2D architecture created by the RSA model. The error between an element length of 0.05mm and 0.0125mm is less than 1% in all cases: 0.27% for 10% Vf, 0.58% for 30% Vf and 0.84% for 50% Vf. An element length of 0.05mm has been used for all subsequent models.

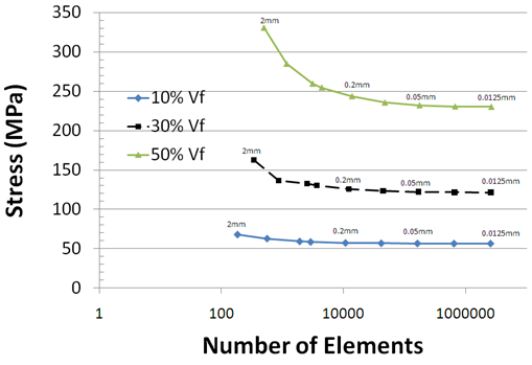


**Fig. 3 Effect of mesh density for three different fibre volume fractions. Numbers inset represent the resin element edge length and the beam length.**

## 6 Decay length of boundary conditions

The critical decay length has been established for a range of models containing different fibre lengths (2.5mm and 10mm), volume fractions (10%, 30%, 50%) and random fibre orientations. The RVE

boundary length was set to two times the fibre length in all cases, as suggested in [16].

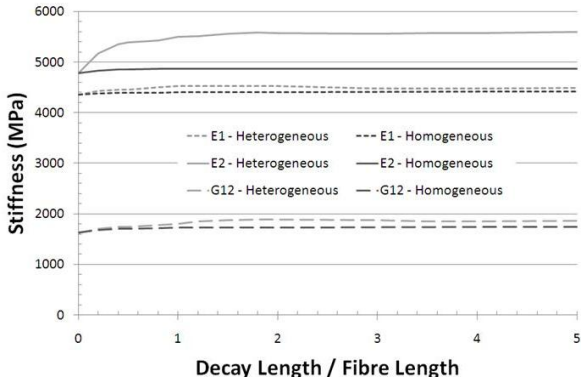


**Fig. 4 Decay length study for two different embedded cell approaches. 10mm fibre length, 10% vf. (Decay length is plotted as a function of fibre length).**

A selection of models is used to evaluate the heterogeneous approach, and this selection is then repeated using the homogeneous approach. The challenge using the homogeneous approach is selecting appropriate material properties for the outer region. For this study they have been obtained from the converged values from the heterogeneous models. Fig. 4 shows how the in-plane stiffnesses vary with increasing decay length ('d') for a model consisting of 10mm long fibres, randomly distributed at a fibre volume fraction of 10% (results are normalised wrt fibre length 'l'). Comparisons are made between the heterogeneous model and the homogeneous model. Table 1 summarises the results for the two approaches, at different fibre lengths and volume fractions. In all cases the homogeneous model converges much quicker than the heterogeneous model, at approximately d/l≈0.5 (d/l≈2 for heterogeneous model) and the CPU time was largely reduced compared with the corresponding heterogeneous model. However, there is an error of up to 13% between the converged values from the two models (E1 – 3.0% error, E2 – 12.9% error, G12 – 9.2% error). This error is independent of fibre volume fraction, but dependent on the fibre length and is generally lower for shorter fibres. The homogeneous model provides a very good approximation for the in-plane stiffnesses for an RVE containing 2.5mm long fibres at 10% vf (E1 – 0.005% error, E2 – 0.006% error, G12 – 0.289% error).

Fig. 5 shows a comparison of stress contours extracted from the inner RVE boundary of both modelling approaches. The images are for the vertical loading case and are taken from the data presented in Fig. 6 at d/l=5. Both models share similar internal features, such as stress concentrations at the bundle ends, but it is clear that there are additional stress perturbations at the RVE boundary for the homogeneous model. When fibre is cropped at the inner boundary for the homogeneous model, an artificial fibre end is introduced, causing a stress concentration in the matrix material. The displaced shape of the homogeneous model is also affected by the local discontinuities, particularly along the top and bottom boundaries.
Whilst the homogeneous model converges at shorter decay lengths compared with the heterogeneous model, accuracy is dominated by the boundary effects around the perimeter of the RVE. Convergence of the heterogeneous model is clearly influenced by the heterogeneity of the surrounding material, but even so, it is considered to be a more reliable approximation because it eradicates the artificial stress concentrations that are present in the homogeneous model.

**Table 1 Error values used to establish convergence of decay length for both heterogeneous and homogeneous approaches. ('d' is decay length and 'l' is fibre length)**

| Heterogeneous | | | | | | | |
|---|---|---|---|---|---|---|---|
| | | Stiffnesses at d/l=2 | | | Error between d/l=2 & 5 | | |
| l | Vf | E1 | E2 | G12 | E1 | E2 | G12 |
| (mm) | (%) | (GPa) | (GPa) | (GPa) | (%) | (%) | (%) |
| 2.5 | 10 | 3.70 | 3.73 | 1.34 | -0.06 | 0.14 | 1.45 |
| 2.5 | 30 | 4.60 | 4.84 | 1.68 | -0.02 | -0.08 | 2.03 |
| 2.5 | 50 | 6.17 | 5.51 | 2.34 | 0.66 | -0.14 | 0.80 |
| 10 | 10 | 4.53 | 5.58 | 1.88 | -0.91 | 0.41 | -0.96 |
| 10 | 30 | 7.54 | 10.20 | 3.67 | -0.29 | 1.78 | 1.52 |
| 10 | 50 | 23.47 | 23.79 | 7.82 | -0.06 | 0.70 | 0.65 |
| Homogeneous | | | | | | | |
| | | Stiffnesses at d/l=0.5 | | | Error between d/l=0.5 & 5 | | |
| l | Vf | E1 | E2 | G12 | E1 | E2 | G12 |
| (mm) | (%) | (GPa) | (GPa) | (GPa) | (%) | (%) | (%) |
| 2.5 | 10 | 3.70 | 3.73 | 1.34 | -0.01 | 0.01 | 0.29 |
| 2.5 | 50 | 5.95 | 5.37 | 2.26 | 0.42 | 0.53 | 1.36 |
| 10 | 10 | 4.39 | 4.86 | 1.71 | 0.55 | 0.09 | 1.54 |

From Fig. 4, all three stiffness values converge after a decay length of two times the fibre length (20mm) for the heterogeneous approach. All three curves plateau at d/l =2 and the error between this point and

d/l=5 is less than 1% for all three stiffness components. Stress contours plotted in Fig. 6 show that a decay length ratio of d/l=2 gives a good approximation of the stress field within the inner RVE boundary. All three plots share similar features, but the magnitude of the stresses around the boundary of d/l=0.5 are generally lower than d/l=2 and d/l=5. The displaced shape for d/l=2 is identical to d/l=5. The edges are not straight and therefore conventional displacement boundary conditions for this RVE model would indeed be inappropriate, which further supports the use of St Venant's principle for heterogeneous materials.

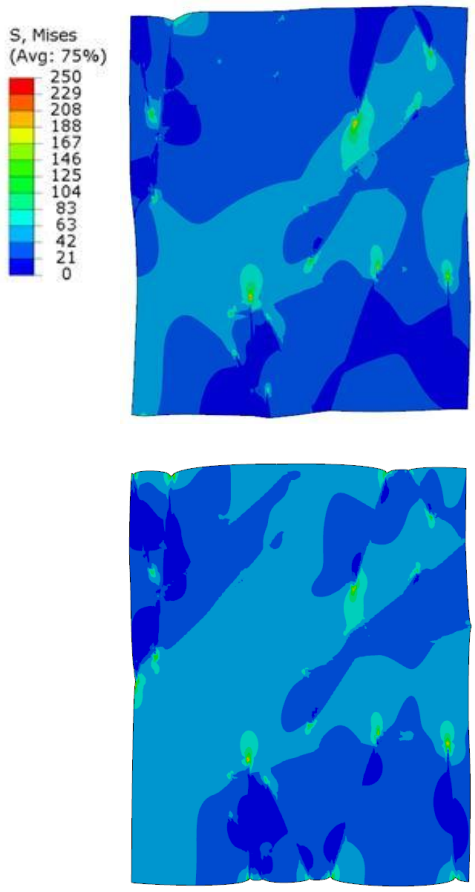


**Fig. 5 Comparison of Von-Mises stress contour plots for an RVE containing 10mm long fibres at 10% vf. Deformed shape from heterogeneous model (top), deformed shape from homogeneous model (bottom).**

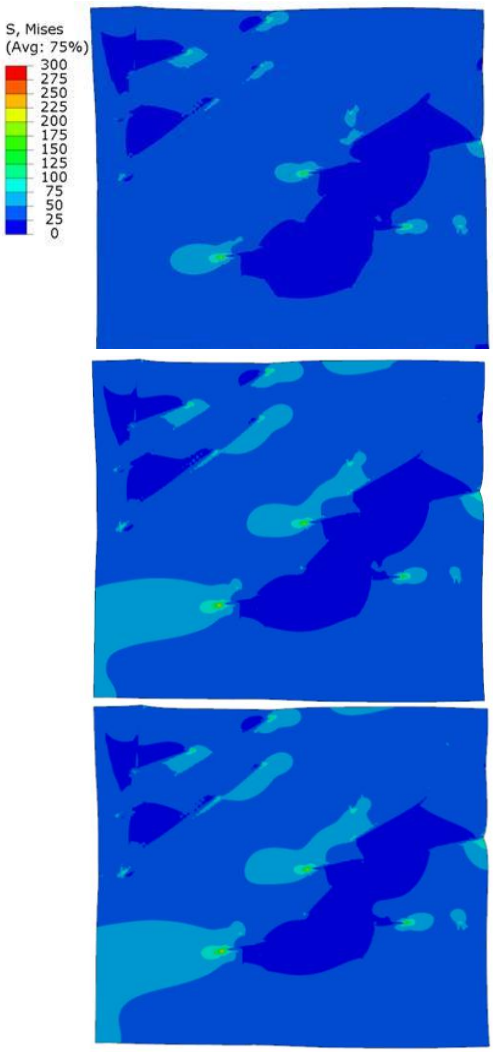


**Fig. 6 Von-Mises stress contours extracted from the inner RVE boundary for three different decay length/fibre length ratios using the heterogeneous approach 0.5 (top), 2 (middle), 5 (bottom). RVE consisted of 10mm long fibres at 10% vf. Loading was in the horizontal direction). Deformation factor was set to 10 and all plots are scaled to the same peak stress of 300MPa.**

Results from a range of other scenarios using the heterogeneous approach show that all errors appear to be ≤2% and the magnitude of the error appears to be independent of fibre length, fibre volume fraction. The critical decay length is therefore found to be two times the length of the fibres in all cases. This observation agrees well with findings in [13], which shows that the critical decay length is two times the length scale of the reinforcing inclusion.

## 7 Conclusions

A novel embedded element technique has been employed to yield simplified FEA meshes for discontinuous fibre composites. A test case has shown that there is less than 1% error between the embedded element approach and a conventional unstructured mesh with coincident nodes at the fibre-matrix interface. Mesh sensitivity studies indicated that the embedded element method was sensitive to the number of fibre bundles within the RVE model.

Random fibre architectures have been created to evaluate the use of different boundary conditions for the heterogeneous fibre architectures. An embedded cell approach has been adopted, whereby the RVE under consideration was embedded into a tertiary material and the effective material properties were extracted from the inner region and two different approaches have been investigates. A critical decay length was found to exist for the both models, over which the effect of incorrectly prescribed boundary conditions applied to the outer boundary of the model became insignificant. The critical decay length for the homogeneous model was found to be ~0.5, however, it was noted that there was a boundary effect between the inner embedded RVE and the host homogeneous region, due to the large stress perturbations present at the bundle ends.

The critical decay length for the heterogeneous approach was found to be 2 times the fibre length in all cases. This resulted in much larger models, but the effective properties extracted from the inner region after convergence were considered to be more reliable than the homogeneous approach.

## References


1. TURNER, T.A., et al., *Low cost carbon-fibre based automotive body panel systems - a performance and manufacturing cost comparison.* Journal of Automobile Engineering - Proceedings of the Institution of Mechanical Engineers Part D, 2008. **222**(1): p. 53-64.
2. HARPER, L.T., et al., *Characterisation of random carbon fibre composites from a directed fibre preforming process: Analysis of microstructural parameters.* Composites Part A: Applied Science and Manufacturing, 2006. **37**(11): p. 2136-2147.
3. FERABOLI, P., et al., *Stochastic laminate anology for simulating the variability in modulus of discontinuous composite materials.* Composites: Part A, 2010. **41**: p. 557-570.
4. WONGSTO, A. and S. LI, *Micromechanical FE analysis of UD fibre-reinforced composites with fibres distributed at random over the transverse cross-section.* Composites: Part A, 2005. **36**: p. 1246-1266.
5. TRIAS, D., et al., *Determination of the critical size of a statistical representative volume element (SRVE) for carbon reinforced polymers.* Acta Meterialia, 2006. **54**: p. 3471-3484.
6. GITMAN, I.M., H. ASKES, and L.J. SLUYS, *Representative volume: Existence and size determination.* Engineering Fracture Mechanics, 2007. **74**: p. 2518-2534.
7. PAN, Y., L. IORGA, and A. PELEGRI, *Numerical generation of a random chopped fiber composite RVE and its elastic properties.* Composites Science and Technology, 2008. **68**(13): p. 2792-2798.
8. HILL, R., *Elastic properties of reinforced solids: some theoretical principles.* Journal of the Mechanics and Physics of Solids, 1963. **11**: p. 357.
9. Luchoo, R., et al., *Net shape spray deposition for compression moulding of discontinuous fibre composites for high performance applications* Plastics, Rubber and Composites, 2010. **39**: p. 216-231.
10. KARI, S., *Micromechanical Modelling and Numerical Homogenization of Fibre and Particle Reinforced Composites*, in *Institute of Mechanics Department*. 2005, Otto-von-Guericke University Magdeburg: Magdeburg.
11. PAN, N., *Analytical characterization of the anisotropy and local heterogeneity of short fiber composites: Fiber fraction as a variable.* Journal of Composite Materials, 1994. **28**(16): p. 1500-1531.
12. Gitman, I.M., H. Askes, and L.J. Sluys, *Representative volume: Existence and size determination.* Engineering Fracture Mechanics, 2007. **74**(16): p. 2518-2534.
13. Wongsto, A. and S. Li, *Micromechanical FE analysis of UD fibre-reinforced composites with fibres distributed at random over the transverse cross-section.* Composites Part A: Applied Science and Manufacturing, 2005. **36**(9): p. 1246-1266.
14. Trias, D., et al., *Determination of the critical size of a statistical representative volume element (SRVE) for carbon reinforced polymers.* Acta Materialia, 2006. **54**(13): p. 3471-3484.
15. Trias, D., et al., *Random models versus periodic models for fibre reinforced composites.* Computational Materials Science, 2006. **38**(2): p. 316-324.
16. Iorga, L., Y. Pan, and A.A. Pelegri, *Numerical characterisation of material elastic properties for random fiber composites.* Journal of Mechanics of Materials and Structures, 2008. **3**(7): p. 1279-1298.